Multiscale Methods for Stiff and Constrained Mechanical Systems

J. M. Sanz-Serna
Departamento de Matemática Aplicada,
Universidad de Valladolid, Valladolid, Spain
sanzsern@mac.uva.es

Gil Ariel,
Department of Mathematics,
The University of Texas at Austin, Austin, TX 78712 USA
ariel@math.utexas.edu

Richard Tsai,
Department of Mathematics,
The University of Texas at Austin, Austin, TX 78712 USA
ytsai@math.utexas.edu

February 11th, 2009

Abstract

We suggest multiscale methods for the integration of systems of second-order ordinary differential equations (ODEs) whose solutions include components that oscillate with large frequencies and small amplitudes. The methods do not need to integrate completely the fast oscillations and may employ step-sizes determined by the rate of change of the slow motions of the system. The technique may be used with any standard ODE method with fixed step-size and also in conjunction with off-the-shelf, variable-step ODE software. Alternatively, the ideas presented here may be used to integrate constrained mechanical systems by means of conventional ODE codes.

1 Introduction

This paper is devoted to the use of Heterogeneous Multiscale Methods (HMMs) [9], [7], [12], [11], [22], [10], [1], [20], [8], [2], [5], [3], [6] (cf. [18]) in the integration of systems of second-order ordinary differential equations (ODEs) whose solutions include components that oscillate with large frequencies and small amplitudes. Such systems arise in Mechanics and other fields of application and are in general costly to inte-

grate numerically, among other things, because standard, explicit algorithms may only operate with step-lengths smaller than the smallest fast period present in the problem. The HMMs suggested here do not need to integrate completely the fast oscillations (micro-scale) and may employ step-sizes determined by the rate of change of the slow motions of the system. Our approach is based on identifying a system of algebraic differential equations (DAEs) approximately satisfied by the slow motions (macro-scale) of the solution; associated with these DAEs there is an underlying system of nonstiff ODEs, which may be integrated by means of any standard explicit ODE solver. Thanks to the HMM methodology, the user does not have to find analytically the underlying system to be integrated: all required information is found numerically by the HMM as the integration proceeds. Alternatively (see Section 5), the methods presented here may be applied to integrate systems of DAEs by means of standard ODE software; the (infinitely stiff) DAE problem is relaxed to a stiff system of ODEs amenable to the HMM approach.

A key difficulty when using HMMs to integrate ODEs stems from the need to relate macro and micro-states. The 'natural' micro-variables (i.e. those in which the micro-model is originally formulated and readily amenable to numerical integration) may not coincide with those fit to describe the slow motions of the macro-scale. A very general HMM technique to cope with this difficulty that may be applied whenever a full set of so-called slow variables is available has been suggested in [1]; this reference also describes an algorithm to identify the required set of slow variables in some classes of ODE systems. The recent contribution [6] focuses on a restricted class of problems; for this class, physical considerations show that the position variables of the given stiff ODEs are slow in the sense of [1], a fact that is then used to formulate simple HMMs that do not provide approximations to the variables that are fast (unsynchronized approach). The present article expands the ideas in [6].

Section 2 contains a description of the class of problems envisaged here. The HMMs are described in Section 3 and tested in Section 4. Our experiments show the way in which off-the-shelf, variable-step numerical ODE software may be used as a HMM macro-integrator. The final Section 5 discusses the scope of the suggested technique.

2 Stiff mechanical problems

We are concerned with systems of ODEs of the form

$$\ddot{\mathbf{q}} = -\omega^2 \sum_{j=1}^{\nu} g_j(\mathbf{q}) \nabla g_j(\mathbf{q}) - \nabla V(\mathbf{q}), \quad 0 \le t \le t_{\max}, \tag{1}$$

where $\mathbf{q}$ is a d-dimensional (column) vector, $\nu \le d$, the real-valued functions g_1, $\ldots$, g_ν, V are smooth and, in the neighborhood of the solution of interest, bounded, along with their derivatives, by constants of moderate size, ∇ denotes the operator $[\partial/\partial q_1, \ldots, \partial/\partial q_d]^T$, and $\omega > 0$ is a large parameter. The initial conditions $\mathbf{q}(0)$, $\dot{\mathbf{q}}(0)$ and the length $t_{\max}$ of the integration interval are assumed to be of moderate size.

A slightly more compact way of writing (1) would be

$$\ddot{\mathbf{q}} = -\omega^2 \mathbf{g}'(\mathbf{q})^T \mathbf{g}(\mathbf{q}) - \nabla V(\mathbf{q}),$$

where $\mathbf{g}$ is the vector-valued function whose ν components are the functions g_j and $\mathbf{g}'$ is the corresponding $\nu \times d$ Jacobian matrix. Note that we are dealing with the Lagrangian system corresponding to the Lagrangian function

$$\mathcal{L} = T - U, \qquad T = \frac{1}{2}\|\dot{\mathbf{q}}\|^2, \qquad U = \frac{\omega^2}{2}\sum_{j=1}^{\nu} g_j(\mathbf{q})^2 + V(\mathbf{q}), \tag{2}$$

and that, typically and due to the large accelerations in the directions of the vectors ∇g_j, the solutions $\mathbf{q}(t)$ will exhibit fast oscillatory behavior with periods of size $O(\omega^{-1})$. It is well known that the numerical integration of (1) may be a difficult task: explicit algorithms suffer from stability restrictions $h = O(\omega^{-1})$ and, moreover, order reductions due to stiffness are likely to manifest themselves [5].

Throughout the paper, our attention is restricted to solutions of (1) for which the total energy $E = T + U$, which is of course a constant of motion, has a bound of moderate size *independent of* ω (cf. the discussion in Section 5). Then, from (2), as $\omega \to \infty$, we have the bounds

$$g_j(\mathbf{q}) = O(\omega^{-1}), \quad j = 1, \ldots, \nu, \tag{3}$$

which imply that any rapidly oscillatory components present in the solution must possess small, $O(\omega^{-1})$, amplitudes (this will be made clearer in the examples below, see also [13], [19]; the functions $\mathbf{q}(t)$ are then slow in the sense of [1] or slow to order 1 in the sense of Kreiss and Lorenz [16]). The numerical methods considered in this article aim at finding the slowly varying components of $\mathbf{q}(t)$ while suppressing the small-amplitude, highly oscillatory components.

Assume that, for each $\omega \gg 1$, $\mathbf{q}_\omega(t)$ is a solution of (1) and that, as $\omega \to \infty$, $\mathbf{q}_\omega(t)$ approaches a limit $\mathbf{q}_\infty(t)$, in such a way that $\dot{\mathbf{q}}_\omega(t) \to \dot{\mathbf{q}}_\infty(t)$, and $\ddot{\mathbf{q}}_\omega(t) \to \ddot{\mathbf{q}}_\infty(t)$.[1] Under these hypotheses, by taking formally limits in (1), we conclude that $g_j(\mathbf{q}) = O(\omega^{-2})$, $j = 1, \ldots, \nu$, and that the limit $\mathbf{q}_\infty$ is a solution of the system of DAEs ([15], [4], [17])

$$\ddot{\mathbf{q}} = \sum_{j=1}^{\nu} \lambda_j(\mathbf{q}) \nabla g_j(\mathbf{q}) - \nabla V(\mathbf{q}) \tag{4}$$

subject to the constraints

$$g_j(\mathbf{q}) = 0, \quad j = 1, \ldots, \nu; \tag{5}$$

here $\lambda_j = -\lim_{\omega\to\infty} \omega^2 g_j$ is the Lagrange multiplier associated with g_j. The initial conditions $\mathbf{q}(0)$, $\dot{\mathbf{q}}(0)$ for this DAE problem have to lie on the constraint manifold of the phase space $(\dot{\mathbf{q}}, \mathbf{q})$ defined by

$$g_j(\mathbf{q}) = 0, \quad \nabla g_j(\mathbf{q})^T \dot{\mathbf{q}} = 0, \quad j = 1, \ldots, \nu. \tag{6}$$

[1] Under this assumption, $\dot{\mathbf{q}}_\omega(t)$ and $\ddot{\mathbf{q}}_\omega(t)$ are bounded independently of ω. Thus $\mathbf{q}_\omega(t)$ is a slow function to order 2 in the sense of [16].

In the language of classical mechanics, the system (4) provides the Lagrange equations of the first kind (i.e. with redundant, nonindependent coordinates) for the holonomic system defined by the Lagrangian (2) and the constraints (5). In this way we have found an ω-independent, index 3, DAE problem whose solutions may be used to approximate the macro-scale of the solutions of the original system of ODEs (1).

In turn, the numerical integration of (4)–(5) may be performed via the so-called underlying system of ODEs

$$\ddot{\mathbf{q}} = \mathbf{g}'^T(\mathbf{g}'\mathbf{g}'^T)^{-1}\mathbf{g}'\nabla V - \mathbf{g}'^T(\mathbf{g}'\mathbf{g}'^T)^{-1}\mathbf{g}''[\dot{\mathbf{q}},\dot{\mathbf{q}}] - \nabla V, \tag{7}$$

obtained by eliminating the Lagrange multipliers; here $\mathbf{g}''[\dot{\mathbf{q}},\dot{\mathbf{q}}]$ denotes the second differential of $\mathbf{g}$ acting on $\dot{\mathbf{q}}$ and we have suppressed the argument $\mathbf{q}$ in $\mathbf{g}'$, $\mathbf{g}''$, ∇V. The $\nu \times \nu$ inverse matrix $(\mathbf{g}'\mathbf{g}'^T)^{-1}$ exists whenever the vectors ∇g_j are linearly independent, i.e. whenever the Jacobian matrix $\mathbf{g}'$ has full rank. Solutions $\mathbf{q}(t)$ of the DAE problem (4)–(5) are also solutions of (7) and, conversely, any solution of (7) *with initial values on the manifold (6)* satisfies (4) and the constraints (5). However (7) also possesses solutions for initial conditions that violate (6); obviously such solutions cannot satisfy (6).

Note that, if the constraints are not linear, then $\mathbf{g}'' \neq \mathbf{0}$ and the velocities $\dot{\mathbf{q}}$ appear in the right hand-side of the underlying system. A consequence of this fact is that (7) is *not*, in general, a Lagrangian system (see below). On the other hand, (7) is *time-reversible*, because the force is an even function of the velocities.

We now present two simple examples to illustrate the preceding considerations.

Example 1: Linear systems. Let S be a $d \times d$ symmetric, positive semi-definite matrix, with normalized eigenvectors $\mathbf{v}_j$, $\|\mathbf{v}_j\| = 1$, $\mathbf{v}_j^T\mathbf{v}_k = 0$, $j \neq k$, and corresponding eigenvalues μ_j^2, $j = 1,\ldots,d$ (multiple eigenvalues are not excluded). It is assumed that ν among the μ_j are $O(\omega)$; more precisely we suppose that there exist constants of moderate size $\kappa_j \geq 0$, $j = 1,\ldots,d$, such that $\mu_j = \kappa_j\omega$, $j = 1,\ldots,\nu$ and $\mu_j = \kappa_j$, $j = \nu+1,\ldots,d$. For simplicity, the eigenvectors $\mathbf{v}_j$ are supposed to be independent of ω.

Since

$$S\mathbf{q} = \omega^2 \sum_{j=1}^{\nu} \big[[(\kappa_j\mathbf{v}_j)^T\mathbf{q}\big](\kappa_j\mathbf{v}_j) + \sum_{j=\nu+1}^{d} \big[(\kappa_j\mathbf{v}_j)^T\mathbf{q}\big](\kappa_j\mathbf{v}_j),$$

the system

$$\ddot{\mathbf{q}} = -S\mathbf{q}$$

is a particular instance of (1) with

$$g_j(\mathbf{q}) = \kappa_j\mathbf{v}_j^T\mathbf{q}, \quad j = 1,\ldots,\nu, \qquad V(\mathbf{q}) = \frac{1}{2}\sum_{j=\nu+1}^{d} \kappa_j^2(\mathbf{v}_j^T\mathbf{q})^2.$$

Each solution $\mathbf{q}(t)$ is a superposition of normal modes:

$$\mathbf{q}(t) \quad = \quad \sum_{j=1}^{d} \alpha_j\mathbf{v}_j\cos(\mu_j t + \theta_j),$$

$$\dot{\mathbf{q}}(t) \quad = \quad -\sum_{j=1}^{d} \alpha_j \mu_j \mathbf{v}_j \sin(\mu_j t + \theta_j);$$

for solutions with energy $E = O(1)$ the bounds (3) imply that the amplitudes α_j of the fast modes $j = 1, \ldots, \nu$ are small, $\alpha_j = O(\omega^{-1})$, but note that the velocities $\alpha_j \mu_j \mathbf{v}_j \sin(\mu_j t + \theta_j)$ of the fast modes undergo $O(1)$ excursions and that the corresponding accelerations are of size $O(\omega)$. Thus these bounded energy solutions $\mathbf{q}(t)$ are slow to order 1 in the sense of [16]): $\mathbf{q}(t)$ and $\dot{\mathbf{q}}(t)$ are bounded independently of ω (the fact that such slow solutions may be characterized by bounds on the energy in the initial condition is an expression of the bounded derivative principle [16]). In terms of the initial data, these solutions are characterized by

$$\mathbf{v}_j^T \mathbf{q}(0) = O(\omega^{-1}), \quad j = 1, \ldots, \nu.$$

On the other hand, smooth solutions (i.e. those that do not include any fast mode[2]) correspond to $\alpha_j = 0$, $j = 1, \ldots, \nu$, or

$$\mathbf{v}_j^T \mathbf{q}(0) = 0, \quad \mathbf{v}_j^T \dot{\mathbf{q}}(0) = 0, \quad j = 1, \ldots, \nu. \tag{8}$$

These satisfy a system of DAEs of the form (4) with the holonomic constraints given by $\mathbf{v}_j^T \mathbf{q} = 0$, $j = 1, \ldots, \nu$. It should perhaps be emphasized that in this example the system of DAEs is satisfied by each smooth $\mathbf{q}(t) = \mathbf{q}_\omega(t)$ with (large but) finite ω and not only by the limiting $\mathbf{q}_\infty(t)$, as it would be the case in more complex situations (for instance if the eigenvectors $\mathbf{v}_j$ were allowed to vary with ω). The Lagrange multipliers λ_j are easily seen to vanish and therefore the underlying system of ODEs (7) reads

$$\ddot{\mathbf{q}} = -\sum_{j=\nu+1}^{d} \big[(\kappa_j \mathbf{v}_j)^T \mathbf{q}\big](\kappa_j \mathbf{v}_j). \tag{9}$$

This is the (unconstrained) Lagrangian system corresponding to the slow potential energy V.

When facing the task of integrating $\ddot{\mathbf{q}} = -S\mathbf{q}$ with initial conditions with moderate energy $E = O(1)$, we may aim at finding the function $\tilde{\mathbf{q}}(t)$ defined by discarding from $\mathbf{q}(t)$ the rapidly oscillatory components: this implies a small, $O(\omega^{-1})$, error in the solution $\mathbf{q}$ but an error of magnitude $O(1)$ in the velocity $\dot{\mathbf{q}}(t)$. In turn $\tilde{\mathbf{q}}(t)$ may be found by numerically integrating the ω-independent associated system of DAEs or the underlying system of ODEs (9). For the DAE, the initial data $\tilde{\mathbf{q}}(0)$, $\dot{\tilde{\mathbf{q}}}(0)$ are obtained by projecting the given initial data $\mathbf{q}(0)$, $\dot{\mathbf{q}}(0)$ onto the manifold defined by (8). For the underlying system, which does not require compatibility of the initial conditions, an *approximate* projection is sufficient.

Example 2: A strong spring in the plane. A unit point mass with coordinates (x, y) moves in a plane. It is attached to one of the extremes of a stiff harmonic spring with unit length and elastic constant ω^2; the other end of the spring is linked to a pivot fixed

[2] In the terminology of [16], such solutions are slow to any order.

at the origin. If $r = (x^2 + y^2)^{1/2}$, the (nonlinear) equations of motion

$$\begin{aligned} \ddot{x} &= -\omega^2(r-1)\frac{x}{r}, \\ \ddot{y} &= -\omega^2(r-1)\frac{y}{r}, \end{aligned}$$

provide a simple instance of (1) with $d = 2$, $\mathbf{q} = [x, y]^T$, $\nu = 1$, $g_1 = r - 1$, $V \equiv 0$, $U = (1/2)\omega^2(r-1)^2$. The problem is best analyzed after changing to polar coordinates:

$$\ddot{r} = -\omega^2(r-1) + r\dot{\phi}^2, \qquad \frac{d}{dt}(r^2\dot{\phi}) = 0.$$

Since the areal velocity $M = (1/2)r^2\dot{\phi}$ is a constant of motion, we may write

$$\ddot{r} = -\omega^2(r-1) + \frac{4M^2}{r^3},$$

so that r varies as the abscissa of a unit point mass under the effective potential $U + 2M^2/r^2$, which possesses a minimum at the root $r_0 > 0$ of the equation

$$\omega^2 r^3(r-1) = 4M^2.$$

Solutions with $E = O(1)$ correspond to

$$r(0) = 1 + O(\omega^{-1});$$

for these solutions, $r(t)$ oscillates with amplitude $O(\omega^{-1})$ and frequency $\approx \omega$ around the value $r_0 = 1 + O(\omega^{-2})$, while $\phi(t)$ evolves with an essentially constant velocity $\dot{\phi}(t) = \dot{\phi}(0) + O(\omega^{-1})$.

Smooth solutions not including fast oscillations have

$$r(0) = r_0, \qquad \dot{r}(0) = 0;$$

for them $r(t)$ and $\dot{\phi}(t)$ remain constant (the tension in the spring exactly balances the centrifugal force so as to have a uniform circular motion). As $\omega \to \infty$, r_0 approaches 1 and we conclude that in our example (4) and (5) take the form

$$\begin{aligned} \ddot{x} &= \lambda\frac{x}{r}, \\ \ddot{y} &= \lambda\frac{y}{r}, \end{aligned}$$

and

$$(x^2 + y^2)^{1/2} - 1 = 0.$$

By eliminating the multiplier λ (that measures the tension in the spring), we arrive at the underlying system

$$\begin{aligned} \ddot{x} &= -\frac{\dot{x}^2 + \dot{y}^2}{r}\frac{x}{r}, \\ \ddot{y} &= -\frac{\dot{x}^2 + \dot{y}^2}{r}\frac{y}{r}, \end{aligned}$$

that may be numerically integrated to obtain approximately the solutions of the original stiff problem. We emphasize that the velocities $\dot{x}$ and $\dot{y}$ appear in the right hand-side of the underlying system and that, furthermore, the system is *not* Lagrangian.

For future reference, note that the fact that the spring has unit length features in the original stiff ODEs and is incorporated through the constraint in the DAE formulation; it is however absent from the underlying ODEs. More precisely, in polar coordinates the underlying system reads $(d^2/dt^2)r^2 = 0$, $(d/dt)r^2\dot{\phi} = 0$: all uniform circular motions, where r and $\dot{\phi}$ remain constant, are possible solutions of this system, regardless of the values of $r(0)$ and $\dot{\phi}(0)$. Moreover, typical solutions spiral with r^2 increasing or decreasing linearly with t; initial conditions for which $r(0) - 1$, $\dot{r}(0)$ are small but non-zero drift slowly away from the constraint manifold $r = 1$, $\dot{r} = 0$ of the DAE.

3 Algorithms

We have just seen how the solutions of the stiff system (1) may be approximated by a numerical integration of the corresponding underlying system (7). The HMMs considered in this paper numerically integrate (7) without any need for analytically determining the actual form of the underlying differential equations to be integrated; the methods just require the knowledge of the original stiff system (1).

3.1 Time stepping

It is convenient to write (1) in first order format

$$\frac{d}{dt}\begin{bmatrix}\mathbf{p}\\ \mathbf{q}\end{bmatrix} = \begin{bmatrix}\mathbf{f}(\mathbf{q})\\ \mathbf{p}\end{bmatrix}, \tag{10}$$

where

$$\mathbf{f}(\mathbf{q}) = -\omega^2 \sum_{j=1}^{\nu} g_j(\mathbf{q})\nabla g_j(\mathbf{q}) - \nabla V(\mathbf{q}),$$

and to proceed similarly for the underlying system (7) that becomes

$$\frac{d}{dt}\begin{bmatrix}\mathbf{p}\\ \mathbf{q}\end{bmatrix} = \begin{bmatrix}\mathbf{F}(\mathbf{p},\mathbf{q})\\ \mathbf{p}\end{bmatrix}. \tag{11}$$

This underlying system is integrated (macro-integration) over the time interval $0 \le t \le t_{\max}$ by means of any standard procedure (macro-integrator), such a Runge-Kutta or linear multistep method. Whenever the macro-integrator requires the evaluation of the right hand-side of (11) at known values $\mathbf{p}^*$, $\mathbf{q}^*$ of the arguments $\mathbf{p}$, $\mathbf{q}$, the upper block component $\mathbf{F}$ is computed by averaging suitable values of the corresponding upper block $\mathbf{f}$ in (10). It is most important to underline that the value $\mathbf{p}^*$ of the lower component of the right hand-side of (11) is known and *must not* be computed via averaging [6]. More precisely, given the values $\mathbf{p}^*$ and $\mathbf{q}^*$, we integrate (micro-integration) in a narrow window $-\eta \le t \le \eta$ the initial value problem defined by (10) and the initial conditions

$$\mathbf{p}(0) = \mathbf{p}^*, \qquad \mathbf{q}(0) = \mathbf{q}^*.$$

The values of the acceleration $\mathbf{f}(\mathbf{q}(t))$ obtained in the micro-integration are then averaged to obtain the required approximate value of $\mathbf{F}$:

$$\mathbf{F}(\mathbf{p}^*, \mathbf{q}^*) \approx \int_{-\eta/2}^{\eta/2} K_\eta(t)\mathbf{f}(\mathbf{q}(t)))\, dt.$$

Here, K_η represents a scaled version

$$K_\eta(\xi) = \frac{2}{\eta} K(\frac{\xi}{\eta/2})$$

of an even, $K(\xi) = K(-\xi)$, weight function or kernel K [11] with unit-mass

$$\int_{-1}^{1} K(\xi)\, d\xi = 1.$$

If η is substantially larger than the periods of the fast oscillations, the rapidly oscillatory components of $\mathbf{f}(\mathbf{q}(t))$ will average to 0 and if η is substantially smaller than the time-scale of the slow components of $\mathbf{f}(\mathbf{q}(t))$, these slow components will not be changed by the averaging procedure. In this way (see the more precise presentation in [20], [6]), it is possible to have a consistent approximation to (11) by sampling, with the help of the micro-integrator, the right hand-side of the given system (10).

3.2 Initial conditions

Given initial conditions $\mathbf{p}(0)$ and $\mathbf{q}(0)$ for (10) subject to the moderate energy condition (3), the initial values to be used in the macro-integration —let us denote them by $\mathbf{P}_0$ and $\mathbf{Q}_0$— are obtained by approximately projecting $\mathbf{p}(0)$ and $\mathbf{q}(0)$ onto the manifold (6). This approximate projection is performed by a micro-integration of (10) with initial data $\mathbf{p}(0)$, $\mathbf{q}(0)$ followed by averaging of the resulting micro-integration solution:

$$\begin{aligned} \mathbf{P}_0 &= \int_{-\eta/2}^{\eta/2} K_\eta(t)\mathbf{p}(t)\, dt, \\ \mathbf{Q}_0 &= \int_{-\eta/2}^{\eta/2} K_\eta(t)\mathbf{q}(t)\, dt. \end{aligned}$$

For the positions $\mathbf{q}$, the solution of the micro-integration oscillates with small $O(\omega^{-1})$ amplitude and fast frequency in the directions transversal to the manifold $g_j(\mathbf{q}) = 0$, $j = 1, \ldots, \nu$ in the configuration space; therefore averaging results in a value $\mathbf{Q}_0$ that approximately lies on this manifold. The same argument applies to $\mathbf{p}$ and the velocity constraints $\nabla g_j(\mathbf{q})\dot{\mathbf{p}} = 0$, $j = 1, \ldots, \nu$.

If the time-interval $0 \le t \le t_{\max}$ for the macro-integration is long, the numerically computed solution of (11) is likely to drift away from the constraint manifold (6) of the DAEs (recall that the underlying system of ODEs does not carry information on the DAE constraints). This difficulty may be softened by periodically projecting the macro-integration solution onto the constraint manifold, a task that may once more

be achieved by micro-integrating and averaging, in exactly the same way as $\mathbf{P}_0$ and $\mathbf{Q}_0$ were obtained from $\mathbf{p}(0)$ and $\mathbf{q}(0)$. This technique amounts to replacing an initial value problem over $0 \leq t \leq t_{\max}$ by a sequence of initial value problems over shorter partial subintervals, in such a way that the final values of $\mathbf{p}$ and $\mathbf{q}$ at a subinterval are taken as initial values for the next subinterval.

4 Numerical experiments

The HMMs described in the preceding section are specified by the choices of the schemes used as macro-integrator and micro-integrator and of the filter function K. All the experiments reported below use the exponential filter function suggested in [11] and are based on the Verlet micro-integrator. Two macro-integrators have been implemented. The first is the 'classical' fourth-order Runge-Kutta formula on a uniform grid with macro-stepsize H. The second is the variable-step Runge-Kutta code *ode45* from the MATLAB suite. We mention that, due to the dependence of the force $\mathbf{F}$ on the velocities $\mathbf{p}$, the system (11) cannot be integrated by the simple Verlet method we use as micro-integrator. Other simple *explicit* methods used in geometric integration [21], [14], [17] have to be ruled out for the same reason. On the other hand, it may be of interest to exploit the time-reversibility of (11) and employ a (more expensive) symmetric, implicit macro-integrator. In this connection it is perhaps useful to point out that, in general, (11) is not a Hamiltonian system and therefore the issue of its symplectic simulation is meaningless.

As a simple test example we have integrated numerically (cf. [13], [19]):

$$\begin{aligned}
\ddot{x}_1 &= -\omega_1^2(r_1-1)\frac{x_1}{r_1} - \omega_2^2(r_{1,2}-1)\frac{x_1-x_2}{r_{1,2}},\\
\ddot{y}_1 &= -\omega_1^2(r_1-1)\frac{y_1}{r_1} - \omega_2^2(r_{1,2}-1)\frac{y_1-y_2}{r_{1,2}},\\
\ddot{x}_2 &= +\omega_2^2(r_{1,2}-1)\frac{x_1-x_2}{r_{1,2}},\\
\ddot{y}_2 &= +\omega_2^2(r_{1,2}-1)\frac{y_1-y_2}{r_{1,2}},
\end{aligned}$$

with

$$r_1 = (x_1^2+y_1^2)^{1/2}, \qquad r_{1,2} = \left((x_1-x_2)^2+(y_1-y_2)^2\right)^{1/2},$$

a system that governs the planar motion of two unit point masses, the first is joined to the origin through a spring of elastic constant ω_1^2 and the second is joined to the first through a second spring of elastic constant ω_2^2. The experiments below successively consider the cases where (i) the first spring is soft and the second hard, (ii) the first spring is hard and the second soft, (iii) both springs are hard.

Although the original cartesian coordinates x_1, y_1, x_2, y_2 were used throughout in the numerical experiments, the *analysis* of the different cases becomes clearer in other coordinate systems, just as our analysis of Example 2 in Section 2 was made easier by turning to polar coordinates. For instance, *in case (i)*, we may describe the configuration of the masses by specifying the abscissa $X = (x_1+x_2)/2$ and ordinate

	RK4						*ode45*
ω_2	H=1	H=1/2	H=1/4	H=1/8	H=1/16	H=1/32	
200	4.3(-1)	6.1(-2)	4.9(-2)	4.8(-2)	4.8(-2)	4.8(-2)	4.9(-2)
500	4.7(-1)	4.6(-2)	9.1(-3)	8.0(-3)	7.9(-3)	7.9(-3)	9.9(-3)
1000	4.7(-1)	4.3(-2)	3.3(-3)	2.1(-3)	2.1(-3)	2.1(-3)	4.1(-3)
2000	4.7(-1)	4.3(-2)	1.7(-3)	6.5(-4)	5.9(-4)	5.9(-4)	2.7(-3)
5000	4.7(-1)	4.1(-2)	1.3(-3)	2.1(-4)	1.5(-4)	1.6(-4)	2.2(-3)
10000	4.6(-1)	3.5(-2)	1.4(-3)	1.3(-4)	6.9(-5)	6.9(-5)	1.9(-3)
20000	3.5(-1)	2.8(-2)	2.1(-3)	1.4(-4)	3.3(-5)	3.1(-5)	1.6(-3)

Table 1: Maximum in the interval $0 \leq t \leq 10$ of the HMM errors in the coordinates $\mathbf{q}$ when $\omega_1 = 1$ and $\omega_2 \gg 1$.

$Y = (y_1 + y_2)/2$ of the center of mass, along with the length $r_{1,2}$ and the attitude angle $\theta = \arctan((y_2 - y_1)/(x_2 - x_1))$ of the second spring. With this choice, it is easily proved that a full set of slow variables in the sense of [1] is given by the four coordinates X, Y, $r_{1,2}$ and θ (in our framework, position variables are always slow, i.e. their time-derivatives are $O(1)$ as $\omega \to \infty$) along with the three velocities $\dot{X}$, $\dot{Y}$, $\dot{\theta}$. The velocity $\dot{r}_{1,2}$ is not slow, as its time derivative behaves like $O(\omega)$. In terms of the cartesian coordinates, all four velocities $\dot{x}_1$, $\dot{y}_1$, $\dot{x}_2$, $\dot{y}_2$ inherit the fast character of $\dot{r}_{1,2}$. Similar analysis may be carried out for cases (ii) and (iii).

(i) The case $\omega_1 = 1$, $\omega_2 \gg 1$. The numerical integrations were carried out in the interval $0 \leq t \leq 10$ and correspond to the initial condition $\dot{x}_1(0) = 1/2$, $\dot{y}_1(0) = -1/2$, $\dot{x}_2(0) = -1/2$, $\dot{y}_2(0) = 1/2$, $x_1(0) = 1$, $y_1(0) = 0$, $x_2(0) = 2 + 1/\omega_2$, $y_2(0) = 0$. Thus initially the kinetic and potential energy equal $1/2$; the true solution presents fast modes due to the initial stretching of the hard spring and to the horizontal components of the initial velocities. The micro-integration used $h = (2\pi/\omega_2)/6$ (so as to place approximately 6 micro-steps in each period of the fast oscillation of the hard spring) and the filtering window width was $2\eta = 20 \times 2\pi/\omega_2$ (so as to cover approximately 20 fast periods).

Table 1 presents the maximum as t varies of the ∞-norm errors in the position vector $\mathbf{q} = [x_1, y_1, x_2, y_2]^T$ with respect to an accurate reference solution of the stiff system computed by means of the *ode45* code with relative error tolerance 10^{-6} and absolute error tolerance 10^{-9}. The parameter ω_2 ranges from 200 to 20000; a variation in the spring constant ω_2^2 of four orders of magnitude. For ω_2 below this range, the HMM errors are large: the problem does not possess the separation between time-scales on which the multiscale methodology is based. For ω_2 above this range, the HMM performs well but the computation of the reference solution becomes prohibitively expensive. Results are reported for the classical RK4 formula with $H = 1, 1/2, \ldots, 1/32$ and for the code *ode45* with the default tolerances (relative 10^{-3}, absolute 10^{-6}). For each fixed value of ω_2, the RK4 errors initially decrease with H and eventually saturate. In fact, while for H large the discrepancy between the HMM solution and the reference solution is due to the global error in the integration of the underlying system with the RK4 formula and to other numerical errors [11], [20], for H small that dis-

	Direct			HMM		
ω_2	Succ.	Failed	Time	Succ.	Failed	Time
200	3563	802	1.6	22	0	1.1
500	8880	2040	4.0	22	0	1.1
1000	17796	4012	8.0	22	0	1.1
2000	35589	7914	15.9	22	0	1.1
5000	88898	19125	39.5	22	0	1.1
10000	178496	38840	76.7	22	1	1.2
20000	350740	80250	157.8	23	1	1.2

Table 2: Statistics of the variable step-size *ode45* integration with default tolerances, $\omega_1 = 1, \omega_2 \gg 1, 0 \leq t \leq 10$; direct integration of the stiff system vs. HMM approach. Columns correspond to numbers of successful and rejected steps and computing time in seconds.

crepancy is due to the difference between the true stiff solution and the solution of the underlying system. Note in this connection that the errors for $H = 1/32$ decrease with increasing ω_2 and that for the larger values of ω_2 they roughly behave as $O(1/\omega_2)$, in line with our earlier discussion in Section 2 of the size of the fast components ignored by the HMMs. We emphasize that, with our definition of h and η, the RK4 runs that correspond to varying ω_2 with a fixed value of H share the same computational effort and that this computational effort is proportional to $1/H$. Thus, the HMM approach becomes more and more appealing as ω_2 increases. Turning now to the *ode45* results reported in Table 1, we see that they are similar to those of RK4 with $H = 1/4$; of course, the use of larger or smaller tolerances has the result of varying accordingly the sizes of the errors.

We next study the cost of the HMM technique in relation with that of a direct integration of the given stiff system. Compiled in Table 2 are some statistics that compare the HMM *ode45* runs in Table 1 with those of a direct integration of the stiff system with *ode45* with *the same values* of the error tolerances, i.e. relative 10^{-3}, absolute 10^{-6} (this *ode45* integration is not to be confused with the one performed to obtain the reference solution). The table clearly shows that, as expected, the computational effort of the direct integration is proportional to ω_2 and that of its HMM counterpart is independent of this stiffness parameter. However, note that, for given values of the tolerances, the results (not reported here) of the direct *ode45* integration do not contain the error implied by suppressing the fast oscillations and are accordingly more accurate than those of the HMM *ode45* code.

Figure 1 depicts the motion of the two masses in the configuration (x, y) plane when $\omega_2 = 500$; solid lines correspond to the HMM *ode45* solution and dots to the reference solution (for both solutions the output of the code was obtained at intervals of length $\Delta t = 0.25$). Figure 2 corresponds to the same run as Figure 1 and shows, as functions of t, the horizontal velocities of the center of mass of the system (i.e. $(\dot{x}_1 + \dot{x}_2)/2$) and of the first and second mass (i.e. $\dot{x}_1$ and $\dot{x}_2$). The discrepancy between the values of $\dot{x}_1$ and $\dot{x}_2$ in the HMM simulation and those in the direct integration

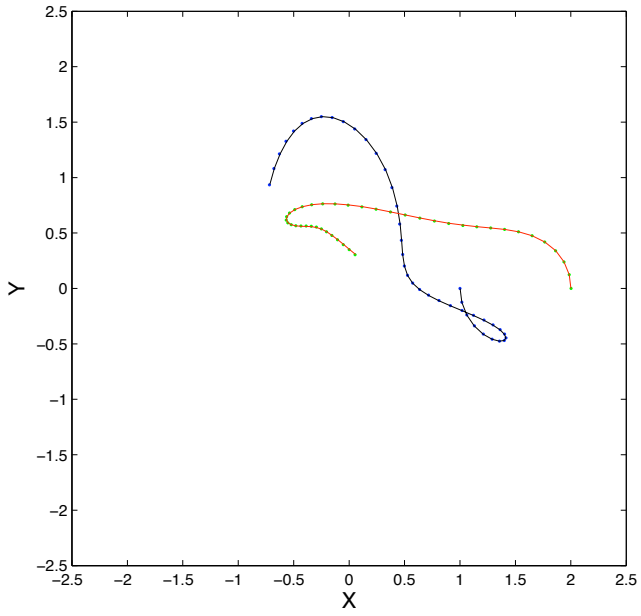

Figure 1: Motion of the point masses in the configuration plane, $\omega_1 = 1$, $\omega_2 = 500$, $0 \leq t \leq 10$, as computed with the *ode45* code with the default tolerances. Dots correspond to the direct integration of the stiff system and the solid line to the HMM simulation.

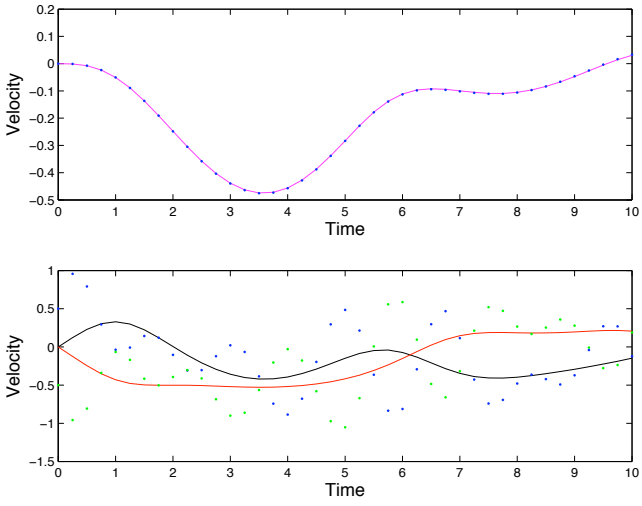

Figure 2: Horizontal velocities of the center of mass (top) and of the individual masses (bottom) for the run in Figure 1.

of the stiff problem is very marked, holds for all values of ω_2 and would not decrease if the error tolerances were made more stringent. As pointed out before, the fast oscillations discarded by the HMM approach have $O(\omega_2^{-1})$ amplitude and $O(\omega_2^{-1})$ period and, as a result, their velocities are of size $O(1)$ (the corresponding accelerations are $O(\omega_2)$). However for the combination $(\dot{x}_1 + \dot{x}_2)/2$, that, as we discussed above, is slow, the HMM solution virtually coincides with that of the direct integration. For a slow variable, the time-derivative is, by definition, of size $O(1)$ and therefore the fast oscillations in $(\dot{x}_1 + \dot{x}_2)/2$ have small $O(\omega_2^{-1})$ amplitude, rather than the $O(1)$ amplitude of the individual velocities $\dot{x}_1$ and $\dot{x}_2$.

(ii) The case $\omega_1 \gg 1$, $\omega_2 = 1$. Experiments analogous to those presented in Table 1 were performed for this case and led to findings similar to those reported above for case (i). Here we show the results of a single run, corresponding to the *ode45* macro-integrator with default tolerances, $0 \leq t \leq 10$ and $\omega_1 = 500$. The micro-integration has $h = (2\pi/\omega_1)/6$, $2\eta = 20 \times 2\pi/\omega_1$, i.e. essentially the same choices we employed before. The initial condition for the velocities is also the same as in (i) above, but this time $x_1(0) = 1 + 20/\omega_1$, $y_1(0) = 0$, $x_2(0) = 2$, $y_2(0) = 0$, so as to have initially a significant amount of potential energy in the hard spring. The maxima in t of the ∞-norm of the errors in the positions and velocities are 0.041 and 19.341 respectively. Figures 3 and 4 show the motion of the masses in the configuration plane and the evolution of the lengths of the springs. Both bear out the suppression of the fast oscillations by the HMM methodology. A warning: there is a stroboscopic effect at work in the figures where the solution is sampled at intervals of length $\Delta t = 0.25$; the fast oscillations are much faster than they appear to be!

(iii) The case $\omega_1 \gg 1$, $\omega_2 \gg 1$. Although other combinations of spring constants were tried successfully, we just quote results with $\omega_1 = \omega_2$. Figure 5 corresponds to $\omega_1 = 500$, $0 \leq t \leq 10$; the initial condition, and the choices of h and η are those used in case (i) above. The macro-integration was, once more, performed with the variable-step code with the default tolerances. Although the HMM is initially capable of following the slow motion of the masses, it becomes completely wrong at $t \approx 2$, when the true motion of the first mass changes from clockwise to anti-clockwise, y_2 attains a minimum and y_1 a maximum. This is an example of the HMM solution drifting away from the constraint manifold; at $t \approx 2$ both springs have become 'numerically' too long, the first stores a potential energy of approximately 3 units (initially the total energy in the system is 1). Figure 6 only differs from Figure 5 in that now the solution has been re-projected, at $t = 1, 2, \ldots, 9$, onto the constraint manifold through the technique described as the end of the preceding Section. This amounts to successively solving ten initial value problems in time-intervals of unit length. The maximum error in the positions x, y is now 0.0359.

The fact that this case appears to be more difficult to integrate than cases (i)–(ii), where re-projections were not needed, is probably attributable to the presence here of two holonomic constraints $r_1 = 1$ *and* $r_{1,2} = 1$ in the limit of infinite stiffness, as distinct from the single constraint $r_1 = 1$ or $r_{1,2} = 1$.

Remark: The accuracy of the micro-integrations. In all the experiments above, the micro-integrations are performed with Verlet's method, with $h = C(2\pi/\omega)$, $\eta = D(2\pi/\omega)$, where C and D remain constant as $\omega \to \infty$. In particular h and η are independent of H in the RK4 runs and of the code tolerances in the *ode45* runs. In

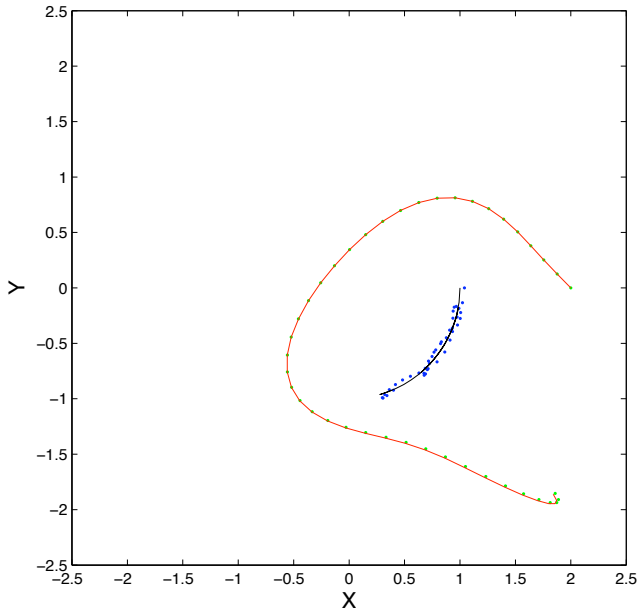

Figure 3: Motion of the point masses in the configuration plane, $\omega_1 = 500$, $\omega_2 = 1$, $0 \leq t \leq T$, as computed with the *ode45* code with the default tolerances. Dots correspond to the direct integration of the stiff system and the solid line to the HMM simulation.

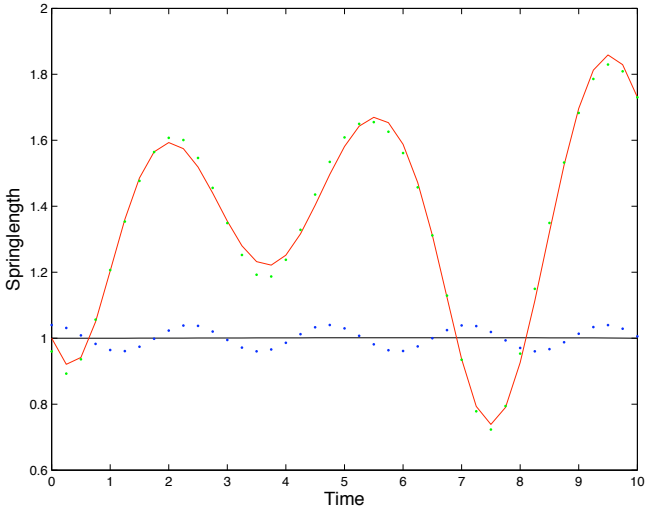

Figure 4: Lengths of the springs as functions of time for the run in Figure 3.

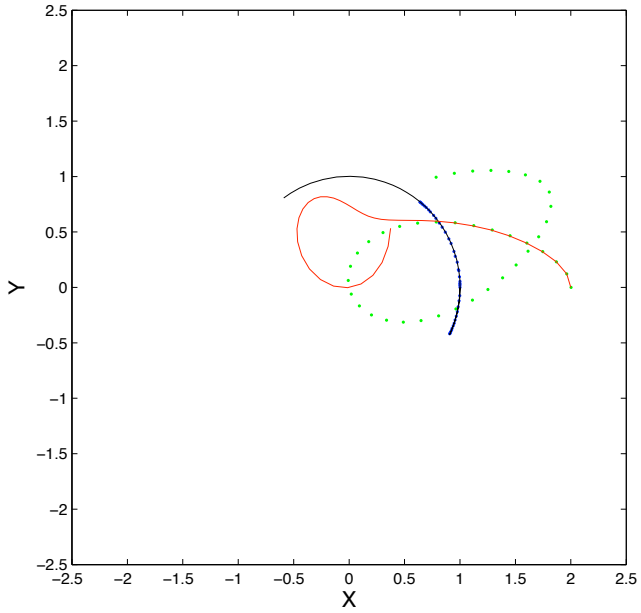

Figure 5: Configuration plane, $\omega_1 = 500$, $\omega_2 = 500$, $0 \leq t \leq T$, *ode45* code with the default tolerances. Dots: stiff system. Solid line: HMM.

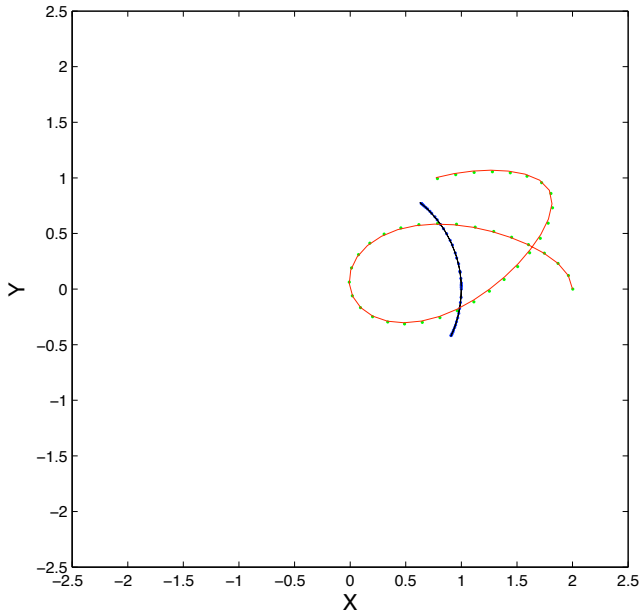

Figure 6: As Figure 5, but now the solution is projected onto the constraint manifold at intervals of length $\Delta t = 1$.

terms of the scaled variable $t' = \omega t$, the derivatives of $\mathbf{q}$ are of order $O(\omega^{-1})$ and the step-length and integration interval are independent of ω. Therefore, see [20], the errors in the values of $\mathbf{q}$ found in the micro-integration are of size $O(\omega^{-1})$, where the constant implied in the O notation decreases when C or D decrease. These errors in $\mathbf{q}$ lead to errors of size $O(\omega^{-1})$ in the slowly varying components of the force $\mathbf{f}(\mathbf{q})$ to be averaged and to errors of size $O(\omega)$ in the fast force components, due to the $O(\omega^2)$ Lipschitz constant. Such large errors have no impact on the performance of the method, because the fast force components are filtered out.

The preceding comments are specific to the format (1) we are considering. In other situations [11], [22], [20], the micro-integrations have to be performed with values of ωh that become smaller as more accuracy is sought, i.e. as the macro-step H (or the tolerance in the macro-integration variable-step code) is decreased.

5 Discussion

We have considered so far the situation where the starting point is the stiff system (1) and the system of DAEs (4) is a means to approximate the non-oscillatory components of the solution we seek. However the roles may be interchanged: it is possible to begin with the system of DAEs and see the HMM integration of (1) as a way to solve the given problem by means of an ODE code. For instance, the integrations in Section 4 may be seen as examples of the use of the code *ode45* from MATLAB to solve DAE problems involving a spring and a rod (cases (i) and (ii)) or two rods (case (iii)); for numerical purposes the rigid rods of the DAE are replaced by stiff springs. Note that it is a simple matter to write the ODE system (1) that corresponds to any given DAE problem (4)–(5).

Although, for simplicity, the exposition has been restricted to stiff systems of ODEs of the form (1), it is clear that many other problems may be catered for with the techniques outlined here. More general formats may include a mass matrix, non-conservative slow forces in lieu of ∇V, slow forces depending on $\dot{\mathbf{q}}$, explicit time-dependence on t, etc. Also the stiff term in (1) could be replaced by

$$\sum_{j=1}^{\nu} \omega_j^2 g_j(\mathbf{q}) \nabla g_j(\mathbf{q}), \quad \omega_1 \gg 1, \ldots, \omega_\nu \gg 1,$$

or by more general expressions.

Perhaps, the main limitation of the technique studied in this paper lies in the required *structure of the solution* q (as distinct from the format of the problem). The requirement that $\mathbf{q}$ may be described as a superposition of a slowly varying function and rapidly varying oscillatory components of *small* amplitude is essential. There are many rapidly oscillatory ODE problems of interest where the solution does not possess such a structure. For instance consider the simple model involving two weakly coupled oscillators:

$$\ddot{q}_1 = -q_1 - \epsilon(q_1 - q_2), \quad \ddot{q}_2 = -q_2 + \epsilon(q_1 - q_2), \qquad \epsilon \ll 1.$$

With the initial conditions $q_1(0) = 1$, $q_2(0) = \dot{q}_1(0) = \dot{q}_2(0) = 0$, the solution is

$$q_1 = \cos(\psi t)\cos t, \quad q_2 = \sin(\psi t)\cos t, \quad \psi = \frac{\sqrt{1+2\epsilon}-1}{2} \approx \frac{\epsilon}{2};$$

the energy, initially in the first oscillator, moves to the second in a time-scale $t = O(\epsilon^{-1})$. After introducing the slow time $\tau = \epsilon t$ and setting $\omega = \epsilon^{-1}$, the system becomes

$$\frac{d^2}{d\tau^2}q_1 = \omega^2 q_1 - \omega(q_1 - q_2), \quad \frac{d^2}{d\tau^2}q_2 = \omega^2 q_1 + \omega(q_1 - q_2), \tag{12}$$

the energy interchange occurs in τ-intervals of length $O(1)$ and the solution

$$q_1 = \cos(\psi^*\tau)\cos(\omega\tau), \quad q_2 = \sin(\psi^*\tau)\cos(\omega\tau), \qquad \psi^* \approx 1/2,$$

oscillates rapidly with period $2\pi/\omega$. In spite of the fact that (12) is not far away from the format (1), the technique suggested in this paper is not applicable, because the fast oscillations have amplitude $O(1)$. (Note that the solution, after the change of independent variable, possesses energy $O(\omega^2)$.)

Acknowledgements. The authors are thankful to Maripaz Calvo and Bjorn Engquist. JMSS research is supported by project MTM 2007-63257, DGI, MEC, Spain. GA and RT are supported by NSF Grant DMS-0714612. RT is also partially supported by an Alfred P. Sloan Fellowship.

References

[1] G. ARIEL, B. ENGQUIST, AND R. TSAI, *A multiscale method for highly oscillatory ordinary differential equations with resonance*, Math. Comput., 78 (2009), pp. 929–956.

[2] G. ARIEL, B. ENGQUIST, AND R. TSAI, *Numerical multiscale methods for coupled oscillators*, Multiscale Model. Simul. , in the press.

[3] G. ARIEL, B. ENGQUIST, AND R. TSAI, *A reversible multiscale integration method*, submitted.

[4] K. E. BRENAN, S. L. CAMPBELL, AND L. R. PETZOLD, *Numerical solution of initial-value problems in differential-algebraic equations*, North Holland, New York, 1989.

[5] M. P. CALVO AND J. M. SANZ-SERNA, *Instabilities and inaccuracies in the integration of highly oscillatory problems*, SIAM J. Sci. Comput., in the press.

[6] M. P. CALVO AND J. M. SANZ-SERNA, *Heterogeneous multiscale methods for mechanical systems with vibrations*, submitted.

[7] W. E. *Analysis of the heterogeneous multiscale method for ordinary differential equations*, Comm. Math. Sci., 1 (2003), pp. 423–436.

[8] W. E, *The heterogeneous multiscale method and the 'equation free' approach to multiscale modelling*, preprint.

[9] W. E AND B. ENGQUIST, *The heterogeneous multiscale methods*, Comm. Math. Sci., 1 (2003), pp. 87–132.

[10] W. E, B. ENGQUIST, X. LI, W. REN, AND E. VANDEN-EIJNDEN, *Heterogeneous multiscale methods: A review*, Commun. Comput. Phys., 2 (2007), pp. 367–450.

[11] B. ENGQUIST AND R. TSAI, *Heterogeneous multiscale methods for stiff ordinary differential equations*, Math. Comput., 74 (2005), pp. 1707–1742.

[12] I. FATKULIN AND E. VANDEN-EIJNDEN, *A computational strategy for multiscale chaotic systems with applications to Lorentz 96 model,* J. Comp. Phys., 200 (2004), pp. 605–638.

[13] B. GARCÍA-ARCHILLA, J. M. SANZ-SERNA, AND R. D. SKEEL, *Long-time-step methods for oscillatory differential equations,* SIAM J. Sci. Comput., 20 (1998), pp. 930–963.

[14] E. HAIRER, CH. LUBICH, AND G. WANNER, *Geometric Numerical Integration, 2nd ed.,* Springer, Berlin, 2006.

[15] E. HAIRER, AND G. WANNER, *Solving Ordinary Differential Equations II, Stiff and Differential-Algebraic Problems, 2nd ed.,* Springer, Berlin, 1996.

[16] H.-O. KREISS AND J. LORENZ, *Manifolds of slow solutions for highly oscillatory problems,* Indiana Univ. Math. J., 42 (1993), pp. 1169–1191.

[17] B. LEIMKUHLER, AND S. REICH, *Simulating Hamiltonian Dynamics,* Cambridge University Press, Cambridge, 2005.

[18] J. LI, P. G. KEVREKIDIS, C. W. GEAR, AND I. G. KEVREKIDIS, *Deciding the nature of the coarse equation through microscopic simulations: the baby-bathwater scheme*, SIAM Rev., 49 (2007), pp. 469–487.

[19] J. M. SANZ-SERNA, *Mollified impulse methods for highly oscillatory differential equations,* SIAM J. Numer. Anal., 46 (2008), pp. 1040–1059.

[20] J. M. SANZ-SERNA, *Modulated Fourier expansions and heterogeneous multiscale methods*, IMA J. Numer. Anal. in the press.

[21] J. M. SANZ-SERNA, AND M. P. CALVO, *Numerical Hamiltonian Problems,* Chapman and Hall, London, 1994.

[22] R. SHARP, Y.-H. TSAI, AND B. ENGQUIST, *Multiple time scale numerical methods for the inverted pendulum problem*, in Multiscale Methods in Science and Engineering, B. Engquist, P. Lötsdedt, and O. Runborg, eds., Lect. Notes Comput. Sci. Eng. 44, Springer, Berlin, 2005, pp. 241–261.